DESIGN AND EFFICIENT IMPLEMENTATION OF OVERSAMPLED GDFT FILTER BANKS FOR SUBBAND ADAPTIVE FILTERING

Stephan Weiß, Moritz Harteneck, and Robert W. Stewart

ABSTRACT

This paper introduces a polyphase implementation and design of an oversampled K-channel generalized DFT (GDFT) filter bank, which can be employed for subband adaptive filtering, and therefore is required to have a low aliasing level in the subband signals. A polyphase structure is derived which can be factorized into a real valued polyphase network and a GDFT modulation. For the latter, an FFT realization may be used, yielding a highly efficient polyphase implementation for arbitrary integer decimation ratios $N \leq K$. We also present an analysis underlining the efficiency of complex valued subband processing. The design of the filter bank is completely based on the prototype filter and solved using a fast converging iterative least squares method, for which we give examples. The design specifications closely correspond with performance limits of subband adaptive filtering, which are under-pinned by simulation results.

1. INTRODUCTION

Subband adaptive filters as shown in Fig. 1 are widely used for problems like acoustic echo cancellation (AEC), where an adaptive system is required to identify very long impulse responses, which becomes viable due to decreased complexity by processing in decimated subbands. However, the case of critical decimation, where the decimation ratio N equals the number of uniform subbands K, requires either cross-terms at least between adjacent frequency bands [3], which compensates the information loss due to non-linear aliasing distortion, or gap filter banks [15, 11], which introduces spectral loss that may not be acceptable. Oversampled filter banks can resolve this problem by introducing spectral redundancy. While complex subband signals can be decimated at any integer rate $N < K$, thus allowing to choose a high decimation rate close to K while suppressing aliasing in the subband signals, for real valued subband signals oversampling is problematic and requires either non-uniform filter banks [6, 5] or single side band (SSB) modulation [1, 13].

Implementation-wise a GDFT filter bank [1] offers several advantages, as it consists of modulated versions of a single prototype filter and can be very efficiently realized, although there is a persistent opinion that polyphase implementations are only viable for integer oversampling ratios $\frac{N}{K} \in \mathbb{Z}$ [1, 8], and usually frequency domain realizations [10] of the filter banks are preferred if larger computational savings for N close to K are to be achieved.

In Sec. 2 an efficient polyphase implementation extended to arbitrary integer decimation ratios $N \leq K$ of a complex valued oversampled generalized DFT (GDFT) is derived based on the work in [2]. Further, we show that complex valued subbands will usually be at least as efficient to process as real ones. Based on the modulation approach, Sec. 3 focuses on the design of oversampled GDFT filter banks, introducing design criteria that also form the performance limitations of subband adaptive filtering in terms of the non-ideal properties of the prototype filter, for which design examples and simulations will be presented in Sec. 4.

S Weiß, M Harteneck and R W Stewart are with Signal Processing Division, Dept. of Electrical and Electronic Engineering, University of Strathclyde, Glasgow, G1 1XW, Scotland, U.K., email: {weiss,moritz,bob}@spd.eee.strath.ac.uk

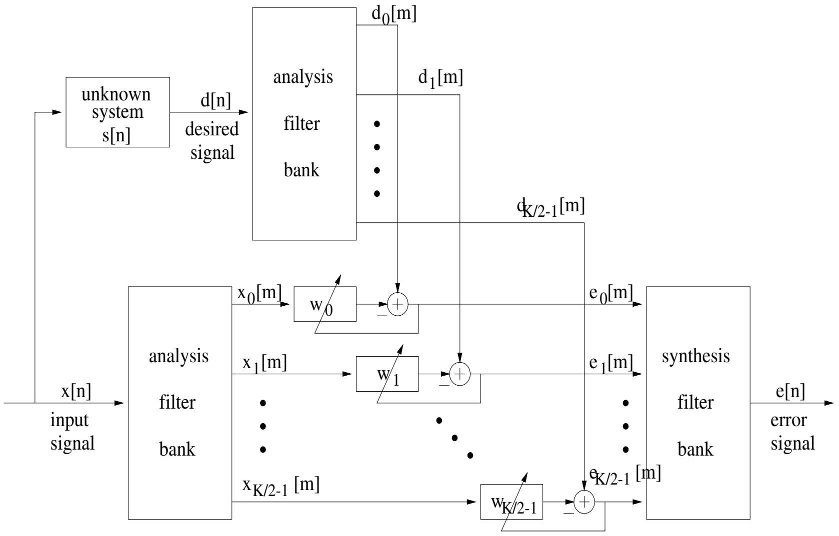

Fig. 1: Subband adaptive filter structure in a system identification setup.

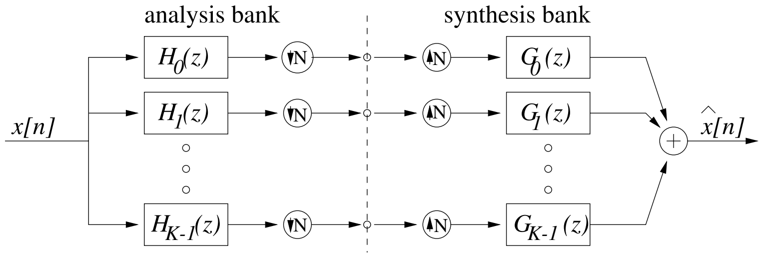

Fig. 2: Analysis and synthesis branch of a K-channel filter bank with subbands decimated by N.

2. COMPLEX SUBBAND DECOMPOSITION BY GDFT FILTER BANKS

2.1. GDFT Modulation

A general structure of a K channel filter bank with decimation by a factor $N \leq K$ is shown in Fig. 2. The analysis filters $h_k[n]$ are derived from a real valued lowpass prototype FIR filter $p[n]$ of even length L_p by a generalized discrete Fourier transform (GDFT),

$$h_k[n] = e^{j\frac{2\pi}{K}(k+k_0)(n+n_0)} \cdot p[n], \qquad k, n \in \mathbb{N}, \tag{1}$$

which can be closely linked to a DCT-IV modulation used for cosine modulated pseudo-QMF $K/2$ channel filter banks [12] by a real operation performed on the complex bandpass filters $h_k[n]$.

The term generalized DFT [1] stems from offsets k_0 and n_0 introduced into the frequency and time indices in the modulation term of (1). Linear phase property of the modulated filters can be ensured by choosing a linear phase prototype filter $p[n]$ and a transform symmetric to $(L_p - 1)/2$ by appropriately setting n_0. A frequency offset $k_0 = \frac{1}{2}$ shifts the bandpass characteristics of the filters $h_k[n]$ and yields the frequency range $[0; \pi]$ to be covered by exactly $K/2$ subbands for an even K, while the remaining subbands are complex conjugate versions and therefore redundant to process, if the input signal to the filter bank is real.

The synthesis filters $g_k[n]$ can be obtained by time reversion and complex conjugation of the analysis filter, i.e. $g_k[n] = \tilde{h}_k[n] = h_k^*[L_p - n + 1]$. Thus, all filters can be derived from one single prototype $p[n]$, which has to be designed appropriately.

2.2. Efficient Filter Bank Implementation

For efficient implementation of the oversampled GDFT filter bank, we employ polyphase representation of the analysis and synthesis filters. Generally, savings due to a polyphase implementation are gained in two steps: first, the calculation of decimated samples will be suppressed; second, computations common to different branches of the analysis or synthesis bank are combined.

2.2.1. Polyphase Representation

With the kth analysis filter written in terms of its N polyphase components $H_{k|j}(z)$, $j = 0(1)N-1$,

$$H_k(z) = \sum_{j=0}^{N-1} z^{-j} H_{k|j}(z^N), \tag{2}$$

a matrix $\mathbf{H}(z)$ with polynomial entries can be created for the analysis filter bank:

$$\mathbf{H}(z) = \begin{bmatrix} H_{0|0}(z) & H_{0|1}(z) & \cdots & H_{0|N-1}(z) \\ H_{1|0}(z) & H_{1|1}(z) & & H_{1|N-1}(z) \\ \vdots & & \ddots & \vdots \\ H_{K-1|0}(z) & H_{K-1|1}(z) & \cdots & H_{K-1|N-1}(z) \end{bmatrix}. \tag{3}$$

With a polyphase decomposition of the input signal $x[n]$, $X(z) = \sum_{j=0}^{N-1} z^{-j} X_j(z^N)$ analogue to (2), and

$$\underline{X}(z) = [X_0(z), X_1(z), \dots X_{N-1}(z)]^T \tag{4}$$

the analysis bank operation can be written as

$$\underline{Y}(z) = \mathbf{H}(z) \cdot \underline{X}(z) \quad , \tag{5}$$

where $\underline{Y}(z) \in \mathbb{C}_{(z)}^{K \times 1}$ contains the K subband signals.

If the polyphase matrix $\mathbf{H}(z)$ is paraunitary, the synthesis of the subband signals may be performed by $\hat{\underline{X}}(z) = \tilde{\mathbf{H}}(z) \cdot \underline{Y}(z)$, where $\tilde{\mathbf{H}}(z)$ is the hermitian of $\mathbf{H}(z)$ with reversed polynomial entries. The reconstructed fullband signal $\hat{x}[n]$ is given in polyphase representation by $\hat{\underline{X}}(z)$. If we combine analysis and synthesis, i.e. $\hat{\underline{X}}(z) = \tilde{\mathbf{H}}(z) \cdot \mathbf{H}(z) \cdot \underline{X}(z)$, perfect reconstructed is characterized by $\tilde{\mathbf{H}}(z) \cdot \mathbf{H}(z) = z^{-L_p+1}\mathbf{I}$, i.e. $\mathbf{H}(z)$ has to be paraunitary [2].

For real input signals $x[n]$, an efficient implementation omits $K/2$ subbands,

$$\hat{\underline{X}}(z) = \text{Re}\left\{\tilde{\mathbf{H}}_r(z) \cdot \underline{Y}_r(z)\right\} = \text{Re}\left\{\tilde{\mathbf{H}}_r(z) \cdot \mathbf{H}_r(z) \cdot \underline{X}(z)\right\}, \tag{6}$$

where the subscript r refers to a reduced matrix representations including only the upper $K/2$ rows of $\mathbf{H}(z)$.

2.2.2. Polyphase Factorization

Let M be the least common multiple (lcm) of the periodicity of the transform in (1), $2K$, and the decimation ratio N, $M = \text{lcm}(2K, N)$, with $\quad M = J{\cdot}2K = L{\cdot}N, \quad J, L \in \mathbb{Z}$. To exploit common calculations between filters, the polyphase components of the analysis filters $\mathbf{H}(z)$ can be written in terms of the M polyphase components of the prototype filter $P(z) = \sum_{m=0}^{M-1} z^{-m} P_m(z^M)$,

$$H_{k|n}(z) = \sum_{l=0}^{L-1} z^{-l} \cdot t_{k,lN+n} \cdot P_{lN+n}(z^L). \tag{7}$$

If the periodicity $2K$ of the transform coefficients $t_{k,n}$ is considered, it is possible to formulate a dense matrix notation

$$\mathbf{H}_r(z) = \mathbf{T}_{\text{GDFT},r} \cdot \mathbf{P}(z) \tag{8}$$

analogue to [2], with the upper half of a GDFT matrix $\mathbf{T}_{\text{GDFT},r} \in \mathbb{C}^{K/2\times 2K}$ and a generally sparse matrix $\mathbf{P}(z) \in \mathbb{R}_{(z)}^{2K\times N}$ with M non-zero polynomial entries

$$\mathbf{P}(z) = [\mathbf{I}_{2K}\ldots\mathbf{I}_{2K}] \cdot \text{diag}\left\{P_0(z^L), P_1(z^L), \ldots P_{M-1}(z^L)\right\} \cdot \begin{bmatrix} \mathbf{I}_N \\ z^{-1}\mathbf{I}_N \\ \vdots \\ z^{-L+1}\mathbf{I}_N \end{bmatrix} . \tag{9}$$

The GDFT transform matrix $\mathbf{T}_{\text{GDFT},r}$ in (8) can be further factorized to yield

$$\mathbf{T}_{\text{GDFT},r} = \mathbf{D}_1 \cdot \mathbf{T}_{\text{DFT},r} \cdot [\mathbf{I}_K\ \mathbf{I}_K] \cdot \mathbf{D}_2, \tag{10}$$

where $\mathbf{D}_1 = e^{-j\frac{\pi}{K}n_0} \cdot \mathbf{I}_{K/2}$ applies a phase correction and $\mathbf{D}_2 \in \mathbb{C}^{2K\times 2K}$ is a diagonal matrix with elements $e^{j\frac{\pi}{K}(n-n_0)}$, $n = 0(1)2K-1$. The representation in (10) allows savings, as $\mathbf{T}_{\text{DFT},r} \in \mathbb{C}^{K/2\times K}$ consists of the upper $K/2$ rows of a K-point DFT matrix with entries $e^{j\frac{2\pi}{K}kn}$, which can be implemented using standard FFT algorithms.

2.2.3. Computational Complexity

Using this polyphase decomposition and factorization to efficiently implement an analysis bank operation, the signal is processed by a real valued polyphase network, $\mathbf{P}(z)$, followed by a complex transformation. On the synthesis side, the subband signals are rotated by a transform, and only their real part again fed into a polyphase network $\tilde{\mathbf{P}}(z)$. Recording computations, both operations result in a computational complexity of

$$C_{\text{bank}} = \frac{1}{N}\left(4K\log_2 K + 6K + L_p\right) \tag{11}$$

real multiplications per fullband sample.

2.3. Complex Vs Real Valued Subband Processing

The ratio of computational complexity between adaptive filtering with real and complex valued subband signals for order $\mathcal{O}(L_a^i)$ algorithms can be derived as

$$\begin{aligned} C_{\text{real}} \ \propto\ L_a^i \qquad &, \quad C_{\text{complex}} \ \propto\ 4 \cdot \left(\frac{1}{2}\cdot\left(\frac{L_a}{2}\right)^i\right) \\ &\longrightarrow \quad \frac{C_{\text{complex}}}{C_{\text{real}}} = \frac{1}{2^{i-1}}. \end{aligned} \tag{12}$$

where L_a is the length of an adaptive filter. Note that the complex case effectively appears with a doubled decimation ratio, resulting in shorter filters and slower update, but requires 4 real multiplications for a complex one. Thus in terms of processing load, $\mathcal{O}(L_a)$ algorithms like LMS and NLMS have same computational complexity for complex and real valued implementations, while for quadratic dependencies ($i = 2$) like the RLS the computational burden can be halved by going complex.

Complex subband processing also doubles the range of possible decimation ratios to choose from $\mathbb{N} \ni N \leq K$ over real valued methods like SSB [1] or non-uniform filter banks [6].

3. PROTOTYPE DESIGN

This section discusses two requirements of the filter bank design, stopband attenuation and perfect reconstruction, which will both be expressed in terms of the prototype filter. Based on this, an iterative least-squares design is presented.

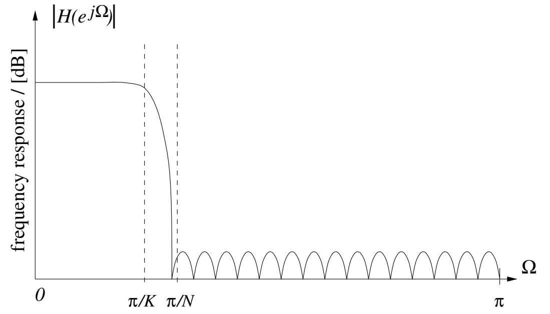

Fig. 3: Required frequency response of a real valued prototype filter $p[n]$ for a $K/2$ channel oversampled modulated GDFT filter bank with decimation by N.

3.1. Stopband Energy

The frequency response of a prototype filter $p[n]$ for a K-channel GDFT bank with decimation by N is shown in Fig. 3. Every frequency of the input signal in the interval $[\pi/N;\pi]$ will be aliased into the baseband after filtering and decimation, and cause a distortion of the subband signal, which can be modelled as additive noise, motivating an SNR measure for white Gaussian input signals [14]:

$$\text{SNR} = \frac{\int_0^{\pi/N} |P(e^{j\Omega})|^2 d\Omega}{\int_{\pi/N}^{\pi} |P(e^{j\Omega})|^2 d\Omega}. \tag{13}$$

The denominator of (13) forms a measure of the stopband energy. It can be numerically approximated using the Eigenfilter method [12], which evaluates the real part of the frequency response in the stopband

$$\text{Re}\{P(e^{j\underline{\Omega}})\} = \mathbf{T}_{\text{DCT}} \cdot \mathbf{p} \tag{14}$$

at discrete frequencies $\Omega_m, m = 1(1)M$ by multiplying the coefficient vector of the prototype, $\mathbf{p} \in \mathbb{R}^{L_p \times 1}$, to a DCT matrix $\mathbf{T}_{\text{DCT}} \in \mathbb{R}^{M \times L_p}$ with entries $t_{m,n} = \cos(n \cdot \Omega_m)$, $n = 0(1)L_p - 1$.

Symmetry of $\mathbf{p}$ is enforced by introducing a permutation matrix $\mathbf{S}_1 = \left[\mathbf{I}_{L_p/2}, \mathbf{J}_{L_p/2}\right]$, where $\mathbf{I}$ and $\mathbf{J}$ are identity and the reverse identity matrices and $\mathbf{b} = \mathbf{S}_1^T \cdot \mathbf{p}$, yielding

$$\text{Re}\{P(e^{j\underline{\Omega}})\} = \mathbf{T}_{\text{DCT}} \cdot \mathbf{S}_1 \mathbf{S}_1^T \cdot \mathbf{p} = \mathbf{T}_{\text{DCT}} \cdot \mathbf{S}_1 \cdot \mathbf{b}. \tag{15}$$

3.2. Power Complementary Condition

If aliasing is sufficiently suppressed, time-invariance of the input-output behaviour of the filter bank system in Fig. 2 is ensured and the near PR condition reduces to the requirement of power complementarity [5, 12],

$$\sum_{k=0}^{K-1} H_k^*(z^{-1}) \cdot H_k(z) \overset{!}{=} z^{-L_p+1}. \tag{16}$$

Exploiting the modulation of the passband filters $H_k(z)$, this requirement is equivalent to demanding

$$\sum_{k=0}^{K-1} P_k^*(z^{-1}) \cdot P_k(z) \overset{!}{=} \frac{1}{K} \cdot z^{-L_p+1}, \tag{17}$$

where $P_k(z)$ are the K polyphase components of the prototype filter $P(z)$ [12]. If the summands on the left hand side are implemented in the time domain by multiplication of a convolutional matrix $\mathbf{P}_k \in \mathbb{R}^{(2Lp/K-1)\times(L_p/K)}$ with a vector $\mathbf{p}_k \in \mathbb{R}^{(Lp/K \times 1)}$ containing the elements of the kth polyphase filter of $p[n]$, (17) becomes

$$\underbrace{[\mathbf{P}_0 \mathbf{P}_1 \ldots \mathbf{P}_{K-1}]}_{\mathbf{V}} \cdot \underbrace{\begin{bmatrix} \mathbf{p}_0 \\ \mathbf{p}_1 \\ \vdots \\ \mathbf{p}_{K-1} \end{bmatrix}}_{\mathbf{v}} = \mathbf{V}\mathbf{S}_2 \cdot \mathbf{p} = \mathbf{V}\mathbf{S}_2\mathbf{S}_1 \cdot \mathbf{b} \overset{!}{=} \underbrace{\begin{bmatrix} \underline{0} \\ 1/K \\ \underline{0} \end{bmatrix}}_{\mathbf{d}} \tag{18}$$

Tab. 1: first three columns: weighting of design criteria and achieved measures according to (19) and (13); right columns: final equivalent fullband model error and reduction in error power for RLS adaptive identification of a delay (all quantities in [dB]).

Prototype Design			Simulation Results	
γ	PRE	SNR	$\|w-s\|_2^2$	$\sigma^2_{dd}/\sigma^2_{ee}$
0	-54.0821	54.9	-54.0153	54.0
30	-34.6191	65.2	-34.6143	66.2
60	-18.0016	77.8	-18.0010	78.5

with a suitable permutation matrix $\mathbf{S}_2 \in \mathbb{N}^{L_p \times L_p}$ that maps the coefficient vector $\mathbf{p}$ onto the polyphase vector $\mathbf{v} = \mathbf{S}_2\mathbf{p}$.

If the subband adaptive filter is free of any other disturbances, the perfect reconstruction error (PRE)

$$\mathrm{PRE} = \|\mathbf{V}\mathbf{S}_2 \cdot \mathbf{p} - \mathbf{d}\|_2^2 \tag{19}$$

gives a limit measure of the achievable accuracy of the equivalent fullband model at the Wiener-Hopf solution [14].

3.3. Iterative Least Squares Design

To fulfill power complementarity and minimize stopband energy, a least-squares problem

$$\mathbf{b} = \arg\min_{\mathbf{b}} \left\| \begin{bmatrix} \mathbf{V}(\mathbf{b})\cdot\mathbf{S}_2\cdot\mathbf{S}_1 \\ \gamma\cdot\mathbf{T}_{\mathrm{DCT}}\cdot\mathbf{S}_1 \end{bmatrix} \mathbf{b} - \begin{bmatrix} \mathbf{d} \\ \underline{0} \end{bmatrix} \right\|_2^2 \tag{20}$$

has to be solved, where γ allows a weighting between both design criteria. The minimization can be performed iteratively [9, 6], solving at each iteration k

$$\mathbf{b}_k = \arg\min_{\mathbf{b}_k} \left\| \begin{bmatrix} \mathbf{V}(\mathbf{b}_{k-1})\cdot\mathbf{S}_2\cdot\mathbf{S}_1 \\ \gamma\cdot\Lambda_\omega\cdot\mathbf{T}_{\mathrm{DCT}}\cdot\mathbf{S}_1 \end{bmatrix} \mathbf{b}_k - \begin{bmatrix} \mathbf{d} \\ \underline{0} \end{bmatrix} \right\|_2^2, \tag{21}$$

where a previous solution $\mathbf{b}_{k-1}$ is substituted to achieve a quadratic approximation of (20). The resulting problem (21) can be easily solved using standard linear algebraic tools [4]. The iteration is stopped when the change from $\mathbf{b}_{k-1}$ to $\mathbf{b}_k$ is below a certain threshold.

Additionally, a diagonal weighting matrix Λ_ω in (21) can be included to improve the stopband attenuation towards the band-edge. Furthermore, a relaxation can be introduced to solve for an intermediate solution $\mathbf{b}'_k$ at step k, from which the final solution is obtained by $\mathbf{b}_k = \alpha\mathbf{b}'_k + (1-\alpha)\mathbf{b}_{k-1}$, for $0 < \alpha \leq 1$.

4. RESULTS

4.1. Design Examples

Fig. 4 shows two prototype filters obtained using the above iterative LS design. The starting coefficients $\mathbf{b}_0$ are calculated by a remez filter design, and for a relaxation $\alpha = 0.5$ the discussed LS method requires 11 iterations to converge in 8.44s CPU time on a Sparc20 workstation. The final PRE and SNR values of the design are listed in Tab. 1.

4.2. Subband Adaptive Filtering Simulations

Using the prototype filters designed in Tab. 1, adaptive system identification of a white Gaussian noise excited delay was performed in subbands. The error terms after convergence of the adaptive filters using the RLS algorithm [7] are also shown in Tab. 1 and closely agree with the properties calculated from the prototype

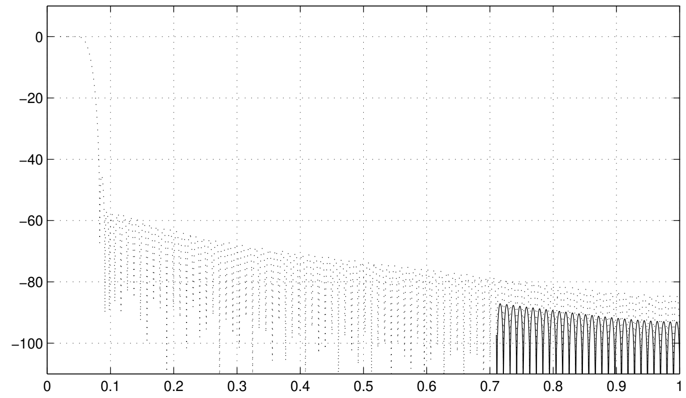
0
−20
−40
−60
−80
−100
0
0.1
0.2
0.3
0.4
0.5
0.6
0.7
0.8
0.9
1